

Annual Review of Pharmacology and Toxicology
From Thalidomide to Rational
Molecular Glue Design for
Targeted Protein Degradation

Vladas Oleinikovas,^{1,*} Pablo Gainza,^{1,*}
Thomas Ryckmans,² Bernhard Fasching,¹
and Nicolas H. Thomä³

¹Monte Rosa Therapeutics AG, Basel, Switzerland; email: bfasching@monterosatx.com

²Ridgeline Therapeutics AG, Basel, Switzerland

³Friedrich Miescher Institute for Biomedical Research, Basel, Switzerland;
email: nicolas.thoma@fmi.ch

ANNUAL
REVIEWS **CONNECT**

www.annualreviews.org

- Download figures
- Navigate cited references
- Keyword search
- Explore related articles
- Share via email or social media

Annu. Rev. Pharmacol. Toxicol. 2024. 64:291–312

First published as a Review in Advance on
August 16, 2023

The *Annual Review of Pharmacology and Toxicology* is
online at pharmtox.annualreviews.org

<https://doi.org/10.1146/annurev-pharmtox-022123-104147>

Copyright © 2024 by the author(s). This work is licensed under a Creative Commons Attribution 4.0 International License, which permits unrestricted use, distribution, and reproduction in any medium, provided the original author and source are credited. See credit lines of images or other third-party material in this article for license information.

*These authors contributed equally to this article



Keywords

molecular glue degrader, MGD, cereblon, CRBN, targeted protein degradation, ternary complex, rational design

Abstract

Thalidomide and its derivatives are powerful cancer therapeutics that are among the best-understood molecular glue degraders (MGDs). These drugs selectively reprogram the E3 ubiquitin ligase cereblon (CRBN) to commit target proteins for degradation by the ubiquitin-proteasome system. MGDs create novel recognition interfaces on the surface of the E3 ligase that engage in induced protein-protein interactions with neosubstrates. Molecular insight into their mechanism of action opens exciting opportunities to engage a plethora of targets through a specific recognition motif, the G-loop. Our analysis shows that current CRBN-based MGDs can in principle recognize over 2,500 proteins in the human proteome that contain a G-loop. We review recent advances in tuning the specificity between CRBN and its MGD-induced neosubstrates and deduce a set of simple rules that govern these interactions. We conclude that rational MGD design efforts will enable selective degradation of many more proteins, expanding this therapeutic modality to more disease areas.

INTRODUCTION

Protein levels in the cell are tightly regulated by the ubiquitin-proteasome system (UPS). Ubiquitin E3 ligases recognize specific structured and intrinsically unstructured elements (degrons) in the target protein, triggering their ubiquitination and degradation by the proteasome. This pathway can be rewired by small molecules, leading to targeted protein degradation of desired novel substrates, commonly referred to as neosubstrates. Perhaps the first example of this mode of action was the serendipitous discovery of thalidomide efficacy in treating symptoms of erythema nodosum leprosum (1), followed by the observation of inhibitory effects on TNF α production (2) and angiogenesis (3), even though the mode of action was unknown at the time. These findings paved the way for the discovery of novel immunomodulatory imide drugs (IMiDs) (such as lenalidomide and pomalidomide) through phenotypic screens and their introduction as a treatment for multiple myeloma (4). The molecular mode of action of IMiDs (5, 6) emerged through determining structures of ternary complexes between E3 ligase, drug, and target (7, 8), which in turn enabled the development of the next-generation mechanism-based drugs.

We now know that IMiDs reprogram the UPS, triggering the recognition and degradation of normally unrecognized proteins (neosubstrates), although some debate remains as to the basal binding affinity of neosubstrate and ubiquitin ligase in the absence of compounds (9). The IMiDs are the first identified members of a growing family of molecular glue degraders (MGDs). Specifically, IMiDs are MGDs that bind to the E3 ligase cereblon (CRBN), creating a new binding surface that can recognize classes of proteins sharing similar degrons. While CRBN is currently the most-studied E3 ligase, the reprogramming of the UPS by small molecules has been extended to ligases such as DCAF15 (10), DCAF16 (11), VHL (12), and DDB1 (13), and other ligase examples are emerging (14). It is now well appreciated that MGDs have the potential to degrade proteins that lack a small-molecule binding site, such as transcription factors, that were historically considered as undruggable. Thus, the potential for MGDs in drug discovery is immense.

This review focuses on CRBN-MGD complexes, the neosubstrates they recognize, and their applications to a variety of disease indications. Moreover, we review patterns in the chemical matter that tune the specificity of CRBN-based MGDs and suggest rational approaches for their design with respect to the degron they are targeting.

CRBN-MGD COMPLEXES RECOGNIZE A STRUCTURAL MOTIF FOR DEGRADATION

The addition of thalidomide, lenalidomide, or pomalidomide to CRBN-containing hematopoietic cell types triggers chemically induced degradation of Ikaros (IKZF1), Aiolos (IKFZ3), or casein kinase 1 alpha 1 (CK1 α), which is facilitated by CRBN (5, 7, 15). The three compounds give rise to overlapping, albeit nonidentical, degradation profiles in cells, yet their targets do not share an obvious protein primary sequence consensus (7). Structural studies, first for CK1 α (16), followed by G1 to S phase transition protein 1 (GSPT1) (17), as well as several zinc-finger (ZF) substrates (8, 15, 16), identified a three-dimensional protein turn, with an invariant glycine, as the shared degron for recruitment by CRBN-MGD complexes (16, 17). This structural E3 ligase-binding motif can be described as an eight-amino-acid stretch with an invariant glycine at the sixth position. In the case of CRBN-MGD complexes, this protein turn is referred to as a G-loop (**Figure 1a,b**), and we refer to each residue position with respect to the invariant glycine (G-5 to G+2).

In structural biology terms, a turn connects two regular secondary structure motifs, thereby changing the direction of the peptide chain. A turn that comprises five residues, with a backbone hydrogen (H) bond between the first (G-4) and fifth (G) positions in the loop, is classified as an alpha-turn. In specific cases, where the turn connects two beta-strands, it is also known as a

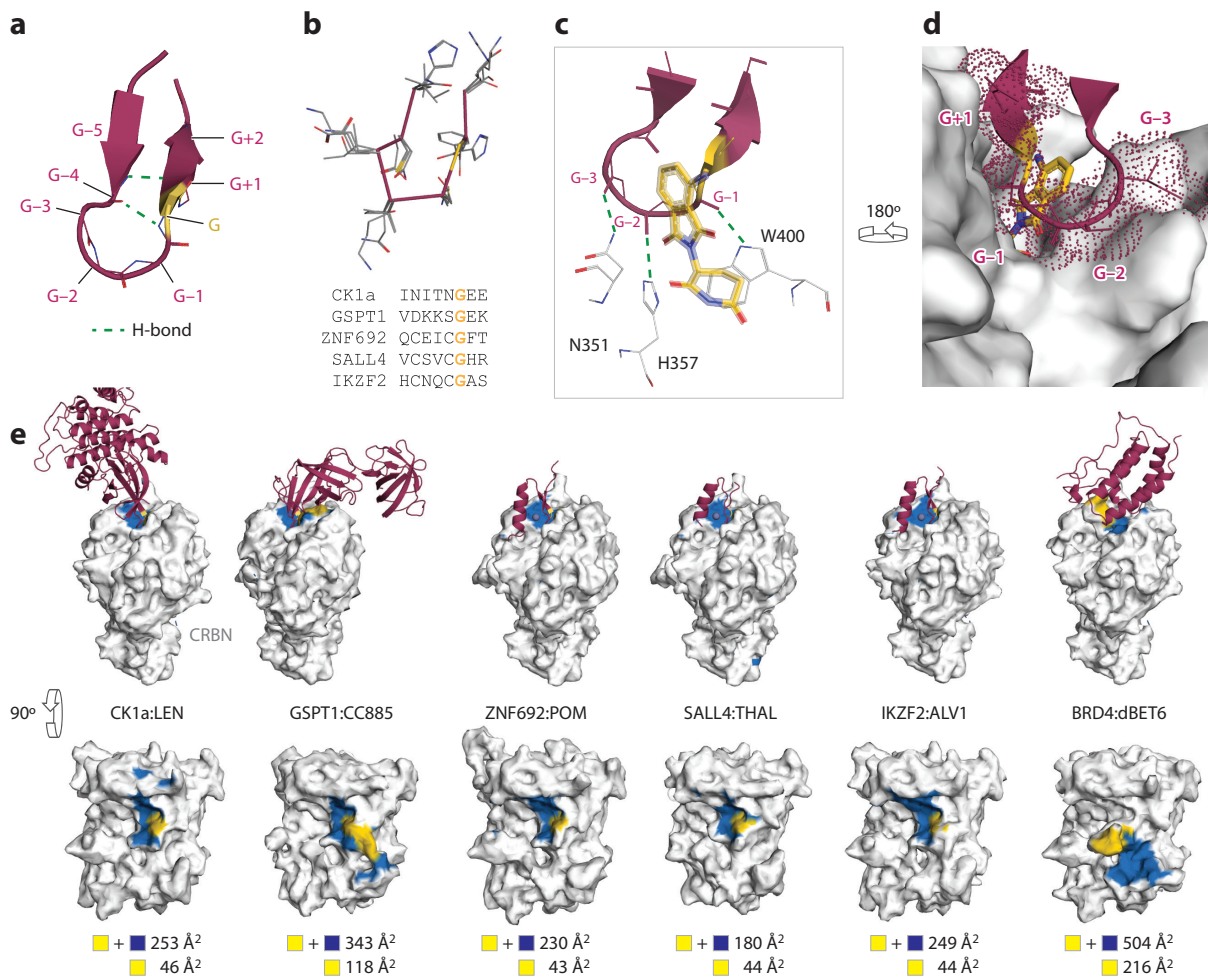


Figure 1

Overview of selected structurally characterized, small-molecule-induced cereblon (CRBN) neosubstrates. (a) Structural model of a G-loop with the invariant glycine (G) residue in gold. (b) Structural alignment of the G-loop of five CRBN neosubstrates, showing the common backbone (maroon) and the sidechains (gray) with the invariant glycine (gold). (c) Hydrogen bonds (green dashes) formed between the alpha-turn of the helix and key residues in CRBN (white), with the drug shown in yellow. (d) Sidechain contacts between G-loop sidechains and CRBN. (e) Structures of CRBN (white molecular surface) with six different neosubstrate–small molecule pairs: CK1 α -lenalidomide (LEN) [Protein Data Bank (PDB) ID 5FQD, <https://www.rcsb.org/structure/5FQD>], GSPT1-CC885 (PDB ID 5HXB, <https://www.rcsb.org/structure/5HXB>), ZNF692-pomalidomide (POM) (PDB ID 6H0G, <https://www.rcsb.org/structure/6H0G>), SALL4-thalidomide (THAL) (PDB ID 6UML, <https://www.rcsb.org/structure/6UML>), IKZF2-ALV1 (PDB ID 7LPS, <https://www.rcsb.org/structure/7LPS>), and, as a reference, the dBET6 PROTAC induced CRBN-BRD4 complex (57). Neosubstrates and the invariant glycine (if present) are colored in maroon and gold, respectively. Each neosubstrate's footprint (i.e., the molecular surface area of the CRBN–small molecule neosurface that becomes buried upon binding of the neosubstrate) is colored in blue and yellow for regions that correspond to the CRBN and small molecule, respectively (below). Each structure is rotated 90° to show the footprint for each neosubstrate, and the neosubstrate is removed for clarity. The area of each footprint is shown below for both the small molecule and CRBN together (yellow + blue) and just compound alone (yellow).

beta-hairpin (18). Both alpha-turns and beta-hairpins are key structural elements of the G-loop in all structurally characterized ternary complexes in the public domain thus far (8, 16, 17, 19–22). The G-loop and the CRBN surface establish three important H bonds between three backbone G-loop carbonyl groups at residues G–3, G–2, and G–1 and the sidechains of CRBN residues Asn351, His357, and Trp400, respectively (**Figure 1c**) (8, 16, 17). The critical role of these sidechain H bonds has been observed in deep mutational scanning studies that identified the respective CRBN residues among the top hot spots for mutation-acquired MGD resistance (23). Hanzl et al. (23) further demonstrate that the CRBN N351D mutant that loses the H bond donor ability no longer degrades GSPT1 in the presence of MGD CC90009, yet it maintains the activity for the BRD4 degrader dBET6 that does not rely on G-loop engagement (23). The change in backbone directionality allows the G-loop to reach deep down into the CRBN pocket, while engaging in favorable van der Waals (vdW) interactions, and in some cases polar contacts, between G-loop sidechains at G–4, G–3, G–2, and G+1 and CRBN (**Figure 1d**). Mutations of the G-loop at positions G–1 and G–3 result in a substantial reduction of CRBN-lenalidomide binding to CK1 α (16). The conserved glycine faces the MGD and engages in favorable vdW contacts (**Figure 1c,d**), and mutational studies found that the glycine position (G) is critical for binding (16).

An important feature of MGD action is that degradation of the target substrate is only observed in the presence of the drug, which renders these substrates neosubstrates. In the absence of the drug, the biochemical interaction between CRBN and the MGD target proteins is weak (9), such that no degradation is detectable (8). The protein-protein interfaces between the G-loop and CRBN are complementary, and some level of residual affinity has been reported. CRBN complexes in the absence of a compound were found to have approximately 4- to 30-fold weaker affinity for IKZF1 and CK1 α , respectively, than in the presence of the IMiD (9). While IKZF1 and CK1 α may engage CRBN in the absence of the MGD (9), they are likely neosubstrates with respect to degradation by CRBN since degradation is only observed in the presence of an MGD (5, 7). However, it is important to point out that the endogenous role of CRBN is only beginning to emerge. For example, CRBN has been implicated in the endogenous degradation of CK1 α (24). In addition, cyclic imides arising from the intramolecular cyclization of glutamine or asparagine residues are chemically reminiscent of IMiDs (25). These have been suggested to form *in vivo* to drive the physiological degradation of target proteins. How these cyclized C termini of endogenous protein targets relate to IMiD-induced targets is currently a matter of intense research.

PROTEIN-PROTEIN INTERACTIONS DRIVE G-LOOP BINDING

In addition to the direct vdW and H bond interactions between the G-loop backbone and CRBN, as well as between the MGD and the G-loop, CRBN engages in additional protein-protein interactions (PPIs) with protein domains of the neosubstrate that extend beyond the G-loop (8, 16, 17, 19, 20) (**Figure 1e**).

These interfaces can be visualized and quantified by their footprint, the region of the CRBN-MGD molecular neosurface that becomes inaccessible to solvent upon binding of the neosubstrate. Although CRBN has been observed in two conformations in structural studies, termed open and closed conformations (8, 22), the closed conformation is believed to be most relevant for neosubstrate recruitment and degradation (22). Thus, here we focus primarily on the closed CRBN conformation. The interaction of a protein (e.g., CRBN) with its partner (e.g., a neosubstrate) can be analyzed from the perspective of its footprint, the molecular surface area of the protein that becomes buried upon engagement of its partner (26). A defining feature of molecular glues is that the MGD footprint is generally substantially smaller than the footprint of the PPI, with the molecular glue mainly stabilizing an interface that already is intrinsically compatible between the

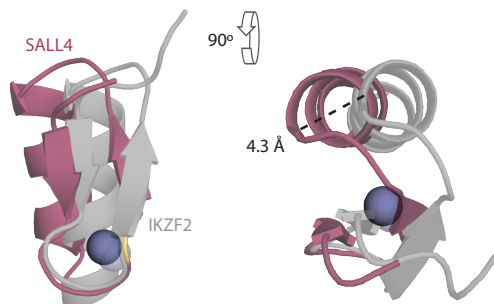


Figure 2

Alternate binding modes of Helios (IKZF2) (*light gray*) and spalt-like transcription factor 4 (SALL4) (*maroon*, with the invariant G-loop glycine in *gold*) to cereblon (CRBN). The structures of IKZF2 [Protein Data Bank (PDB) ID 7LPS, <https://www.rcsb.org/structure/7LPS>] and SALL4 (PDB ID 6UML, <https://www.rcsb.org/structure/6UML>) cocrystallized with CRBN were aligned with respect to the CRBN protein, reflecting a differentiated binding mode for the two zinc fingers (ZFs).

proteins. A typical footprint for a protein involved in a transient PPI is around 400 Å² (26). The footprint between CRBN and its neosubstrates, on the other hand, is smaller, ranging from 180 Å² for the CRBN-thalidomide-SALL4 complex to 343 Å² for the CRBN-CC885-GSPT1 complex (**Figure 1e**). The size of the MGD contribution to this neosurface footprint only ranges from 40 to 118 Å².

THE CRBN-MGD COMPLEXES WITH THE CYS₂-HIS₂ ZF FAMILY

The detailed structural and functional interplay between neosubstrate G-loop, CRBN, and MGD is best understood for ZFs (8). Most known ZF substrates targeted by CRBN-MGD complexes belong to the Cys₂-His₂ (C2H2) subfamily, comprising a beta-hairpin followed by an alpha helix (**Figure 2**). C2H2 ZFs are stabilized by a central Zn²⁺ ion coordinated by two histidine residues originating from the helix together with two cysteine residues located in the beta-hairpin. In C2H2-type ZFs, the two Cys residues are spaced two to four residues apart, yet all known CRBN-engaging ZFs thus far reported have a two-amino-acid spacing (CXXCG motif) with an H bonding pattern consistent with an alpha-turn. Importantly, approximately 73% of C2H2 ZFs in the human proteome contain a CXXCG motif consistent with a G-loop, and thus a total of nearly 5,000 C2H2 ZFs assume a backbone structure principally compatible with CRBN-MGD binding.

To date, seven CRBN-MGD-ZF complexes have been dissected structurally and mechanistically (8, 19–22). In addition to immediate backbone interactions between the ZF, CRBN, and the MGD, all known C2H2 ZF structures show prominent protein-protein interactions at the interface between the G-loop and the ZF alpha helix. While the observed alpha-turn backbones are virtually identical in all of these ZF structures, the detailed residues at the CRBN interface differ, resulting in slightly different ZF binding conformations. This is most evident in an approximately 15° difference in the angle between CRBN and the ZF of IKZF2 compared to that of SALL4 (19) (**Figure 2**).

The available evidence suggests that for some ZF neosubstrates, the neighboring ZF can also interact with CRBN (8). For example, binding of IKZF1 ZF2 to CRBN is more than tenfold weaker than that of a construct of IKZF1 with ZF2 and ZF3 combined (8). Adding an N-terminal IKZF1 ZF1 to ZF2, giving rise to a ZF1-ZF2 fusion construct, does not improve binding, while replacing the C-terminal ZF3 with that of IKZF1 ZF1, resulting in a ZF2-ZF1 protein, gives

only an approximately sixfold increased affinity compared to ZF2 alone (8). Unlike IKZF1 ZF2 alone, neither IKZF1 ZF1 nor ZF3, when assayed in isolation, binds the CRBN-MGD complex. Taken together, this suggests that IKZF1 ZF2 provides the main binding site for the CRBN-MGD interaction and that C-terminal IKZF1 ZF3 plays an auxiliary role (8). A related observation has been made also for SALL4, where the auxiliary ZF in this case appears on the N-terminal end of the main compound-interacting ZF (27). The structural basis underlying dual ZF binding to CRBN is unclear at present.

HOW MANY G-LOOPS ARE THERE IN THE HUMAN PROTEOME?

All available G-loop structures show an almost invariant alpha-turn backbone architecture that occurs frequently within other C2H2 ZFs, as well as in other proteins in the human proteome (**Figure 3**). Because the CRBN E3 ligase complex is present in most tissues, this presents a unique drug discovery opportunity and raises the question, how many different G-loop targets can be degraded by CRBN-MGD neosurfaces?

Surveying human protein structures, alpha-turns are not as common as beta-turns (containing three peptide bonds between secondary structure elements) or gamma-turns (containing two peptide bonds). To estimate the number of potentially suitable G-loops/alpha-turns, we examined the recently released AlphaFold2 (AF2) structural models of the human proteome (28, 29). After extracting an eight-amino-acid stretch containing the G-loop of GSPT1 (residues 570–577) and structurally aligning the backbone of this fragment to the backbone of all consecutive eight-residue fragments in 23,390 structures from AF2 models, we identified 24,865 human protein fragments that align with an RMSD of less than 1.0 Å. From this set, 12,589 have a Gly in the G position. If we add a further condition that a potential G-loop must be surface exposed, this number reduces to 8,692 G-loops, contained in 2,550 human proteins (**Figure 3**). An analysis of which protein domains harbor such a G-loop across the 2,550 human proteins (**Figure 3**) identifies the C2H2 ZF clade as the most prevalent domain class. However, approximately 80% of G-loops are present in proteins that do not contain a C2H2-ZF motif and can be found across diverse protein folds and fold families (**Figure 3**).

THE G-LOOP IS A KEY DETERMINANT OF SPECIFICITY

A conserved structural motif is thus recognized by CRBN-MGD complexes, with hundreds of exposed, structurally conserved G-loops in the human proteome, yet mass spectrometry studies (e.g., see 5) as well as different reporter assays (e.g., see 30) suggest that CRBN-based MGDs have multiple substrates in a given cell type, but not hundreds or thousands? How can this be reconciled? Or in other words, what determines specificity?

Four experimental observations suggest a possible answer: First, the limited number of molecular glues used in studies in the literature preferentially induces the detectable recruitment of only a small number of neosubstrates, as has been observed with AirID (30). Other potential neosubstrates would likely emerge with larger, more diverse MGD libraries. Second, the structure-activity relationship (SAR) governing neosubstrate binding to CRBN-MGD is unusual in that only top binders are preferentially degraded (8). Third, although only a few selected proteins appear degraded in each cell line, or tissue, many other G-loop-containing proteins nonetheless bind to the CRBN-MGD interface (8). Finally, subtle differences at the MGD–target protein or CRBN–target protein interface can convert binders to degraders and vice versa (8, 20).

Evidence for the unusual relationship between affinity and degradation first came from studies of Helios (IKZF2), which differs in the G-loop sequence of ZF2 from IKZF1 in a single, conservative, amino acid change: IKZF1 His146 to Gln (5). While this mutant fully ablated IKZF2

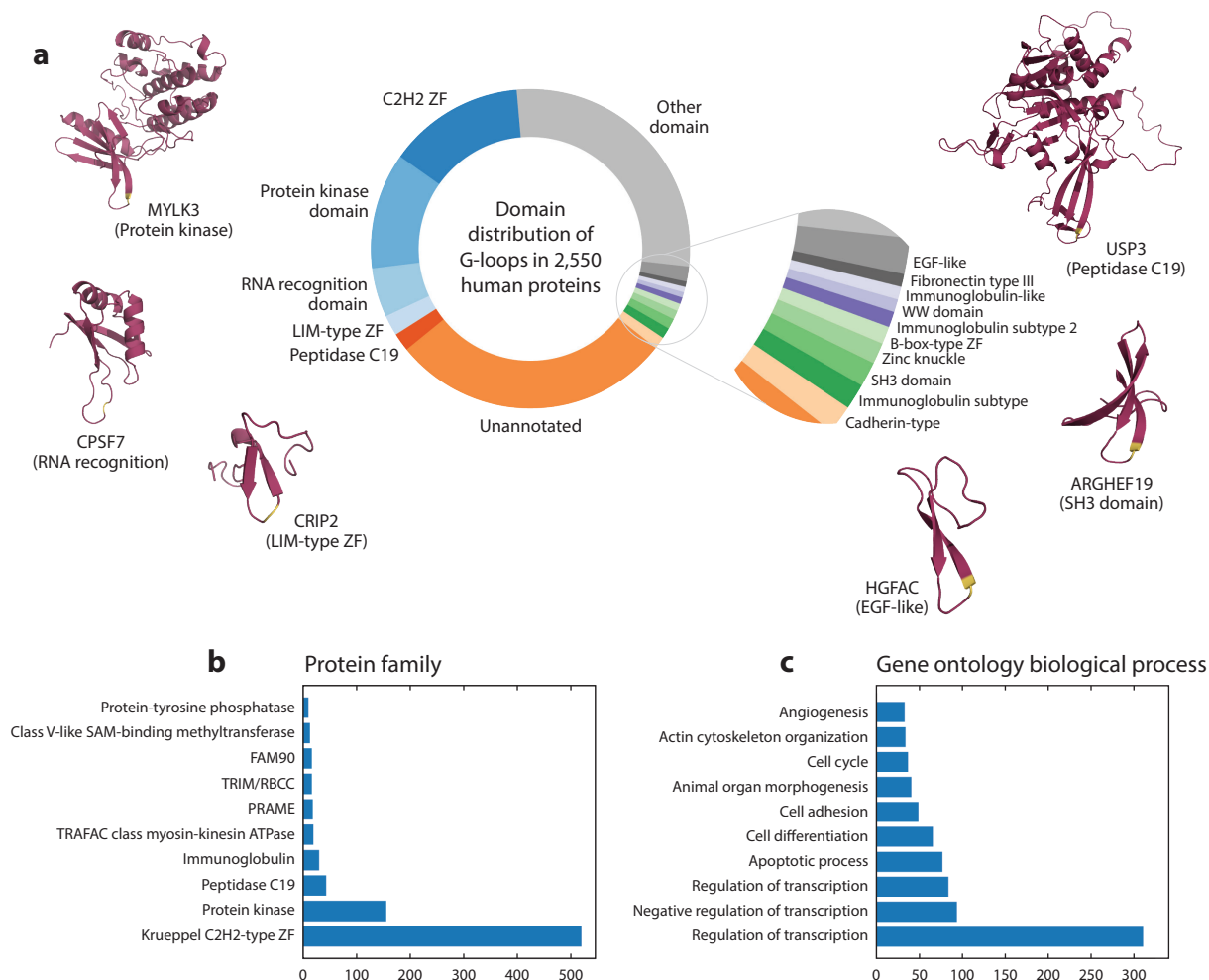


Figure 3

Prevalence of G-loops across human proteins based on AlphaFold2 models. The RMSD between the backbone atoms of each eight-residue fragment in the AlphaFold2 database of protein structures versus the G-loop of GSPT1 was computed. All fragments with a glycine in the sixth position and an RMSD of less than 1.0 Å were considered as G-loops. (a) The plot shows the distribution of G-loops across 2,550 proteins where, for each protein, only the domain G-loop with the lowest RMSD was considered. A selected number of representative folded domain structures are shown, with the domain in maroon and the invariant G-loop glycine in gold. For each gene, the name of the protein is shown, with the protein domain class indicated in parentheses below. (b–c) Histograms show the distribution of a subset of these 2,550 proteins across (b) protein families and (c) gene ontology groupings. Abbreviations: C2H2, Cys2-His2; RMSD, root mean square deviation; ZF, zinc finger.

degradation by pomalidomide or lenalidomide (5), it only reduced in vitro binding by two- to threefold (8). A similar dependency, a relatively minor loss in binding resulting in a dramatic change in degradation efficiency, was also evident when mutating surface residues in CRBN. Mutating Val388 to Ile in human CRBN renders it closer to the mouse protein, and it no longer supports the degradation of IKZF1. This mutant protein exhibited only a threefold loss in binding compared to wild-type human CRBN (16). Analogously, human CRBN degrades human CK1 α with the help of lenalidomide, yet pomalidomide seemed ineffective in cellular degradation,

even though it showed only twofold less binding. While there is, to our knowledge, not a single biophysical parameter (affinity, off rate, etc.) that can reliably predict cellular degradation at this time, it seems increasingly likely that only the best binders drive degradation (8, 16, 17, 31). Consequently, other G-loop-containing proteins may engage the CRBN-MGD neosurface already, sharing a similar G-loop conformation, but without sufficient strength to drive degradation. If true, it could imply that small changes in binding of those neosubstrates already engaged at the MGD-CRBN interface may turn binders into degraders, and that small binding differences *in vitro* are magnified in cells, giving rise to defined degradation hierarchies among neosubstrates.

The first direct proof of this hypothesis came from studies examining the degradation of ZF-containing proteins (8). C2H2 ZFs are mostly invariant in backbone structures yet vary broadly in sequence along the G-loop. Correlating structural and protein-docking calculations with biochemical binding data and cellular degradation reporters demonstrated that many more ZFs appear to bind than are degraded (8). Reporter degradation screens with a single ZF fused to green fluorescent protein (GFP) found 11 ZFs degraded, and computational structural biology tools then identified 17 additional neosubstrates that successfully engaged CRBN yet showed no cellular reporter degradation (8). Changing the MGD, on the other hand, illustrated that some of those nondegrading binders could be converted to degraders by virtue of changing the chemistry of the compound, hence fine-tuning neosubstrate binding to CRBN. Sievers et al. (8) hypothesized that 200–500 ZFs may have a structural degron compatible with CRBN-MGD binding with standard MGDs such as pomalidomide, and that this number likely includes more members once the chemical scaffold of the MGD changes away from the classical thalidomide scaffold. Those proteins that already show binding to CRBN-MGD complexes are more easily primed for being converted into degraders. This was subsequently shown for the bound, yet not degraded, C2H2 members Helios (20) and ZBTB16 (32), where structural modifications in the MGD demonstrated selective degradation.

EVEN MORE CRBN-MGD TARGETS

With hundreds of proteins potentially binding to CRBN with traditional MGDs such as thalidomide, lenalidomide, or pomalidomide, the number of reported MGD-induced CRBN binders has grown steadily over the years, with CRBN-directed small-molecule libraries now continuously expanding. Yet defining those proteins that are direct targets of CRBN-MGDs has remained challenging. Some of the reported binders are likely true neosubstrates (i.e., directly degraded), while others may be weak binders with no degradation. Reported binders from chemical proteomics degradation assays, on the other hand, revealed dozens of targets degraded with monovalent compounds; while some of these are direct targets, most are only indirectly affected (33). Likewise, proximity ligation assays, where an overexpressed CRBN is fused to a biotinylating enzyme, expanded the scope of potential targets, including those that only show weak affinity without any signs of degradation (30). This assay identifies direct degradation targets, as well as bound yet nondegraded targets, in addition to proteins that are only in close proximity to the CRBN-MGD complex but are not directly targeted by the ligase at all. An analysis of the literature identified 49 potential neosubstrates (**Table 1**). Some of these, such as RAB28 (5), FAM83F (27), or FAM83G (33), do not have an obvious G-loop and could be indirect substrates that exist in a complex with a direct target. FAM83F and FAM83G, for example, are known interactors of CK1 α (33). Of the 49 reported neosubstrates or weak binders, 28 are C2H2 ZFs and contain at least one C2H2 ZF with a G-loop. The prevalence of ZF targets is somewhat expected given that approximately 3% of the human proteome contains at least one C2H2 ZF compatible with CRBN-MGD binding. These C2H2 neosubstrates include WIZ (27), SALL4 (19), and ZBTB16 (32). Remarkably, Thompson and colleagues (32) demonstrate that, depending on the nature of the MGD, ZBTB16 can be

Table 1 Cereblon neosubstrates reported in the literature

Protein name	G-loop ^a	Domain comment	RMSD ^b	Reference(s)
IKZF1/3	Yes	C2H2 ZF	0.555	5, 15
RAB28	No	Other	>1	5
CSNK1A1	Yes	Kinase	0.509	7
GSPT1	Yes	Beta-barrel C-T domain	0.602	17
GSPT2	Yes	GSPT1 homolog	0.603	58
ZFP91	Yes	C2H2 ZF	0.558	8
DTWD1	Yes	DTW domain	0.697	27
RNF166	Yes	C2HC RNF-type and RING-type ZF	0.604	27
ZNF692	Yes	C2H2 ZF	0.580	8
ZNF276	Yes	C2H2 ZF	0.617	8
ZNF653	Yes	C2H2 ZF	0.615	8
ZNF827	Yes	C2H2 ZF	0.619	8
BCL6	Yes	C2H2 ZF	0.419	8
BCL6B	Yes	C2H2 ZF	0.345	8
ZBTB7B	Yes	C2H2 ZF	0.627	8
HIC2	Yes	C2H2 ZF	0.609	8
EGR1	Yes	C2H2 ZF	0.643	8
OSR1	Yes	C2H2 ZF	0.585	8
SALL3	Yes	C2H2 ZF	0.608	8
OSR2	Yes	C2H2 ZF	0.585	8
SALL1	Yes	C2H2 ZF	0.656	8
SALL4	Yes	C2H2 ZF	0.594	27
GZF1	Yes	C2H2 ZF	0.580	27
ZBTB39	Yes	C2H2 ZF	0.581	27
ZNF98	Yes	C2H2 ZF	0.591	27
WIZ	Yes	C2H2 ZF	0.563	27
FAM83F	No	Other	>1	27
PATZ1	Yes	C2H2 ZF	0.558	59
TP63	Yes	p53, DNA-binding domain	0.618	31
PLK1	No	Kinase	>1	60
ZBTB16	Yes	C2H2 ZF	0.586	32
BNIP3L	No	Disordered with BH3 domain	>1	61
CYP19A1	No	Aromatase	>1	62
ARID2	No	Other	>1	63
IKZF2/4	Yes	C2H2 ZF	0.596	20
ZNF654	Yes	C2H2 ZF	<1	37
HBS1L	Yes	GSPT1 structural homolog	0.734	64
ZMYM2	Yes	MYM-type ZF	0.646	34
CDK4	Yes	Kinase	0.641	65
ZKSCAN5	Yes	C2H2 ZF	0.561	35
eIF3i	Yes	WD beta-propeller domain	>1	66
PDE6D	Yes	Phosphodiesterase	0.559	34
FAM83G	No	Other	>1	30
ZNF687	Yes	C2H2 ZF	0.583	30

(Continued)

Table 1 (Continued)

Protein name	G-loop ^a	Domain comment	RMSD ^b	Reference(s)
MYH9	Yes	SH3 domain	0.540	30
DIDO1	No	PHD ZF	>1	30
ZNF536	Yes	C2H2 ZF	0.603	30
ZNF687	Yes	C2H2 ZF	0.583	30
GATAD2A	No	GATA-type ZF	>1	30

^aThe presence of a G-loop that aligns within a 1.0-Å RMSD to the *GSPT1* G-loop in respective AF2 models.

^bRMSD of the best G-loop in the AF2 model to the G-loop in *GSPT1*.

Abbreviations: AF2, AlphaFold2; C2H2, Cys2-His2; PHD, plant homeodomain; RMSD, root mean square deviation; WD, tryptophan aspartic acid; ZF, zinc finger.

targeted for degradation with two distinct binding modes that primarily engage G-loops on different ZF domains. Other ZFs beyond the C2H2 ZF family may be druggable as well, as the protein ZMYM2, a MYM-type ZF, which contains a G-loop at Gly429, was also shown to confer CRBN-dependent degradation in response to avadomide (34). Beyond proteins with ZFs, numerous other CRBN neosubstrates have been reported, such as PDE6D (34), a phosphodiesterase that contains a G-loop around Gly28 (Table 1).

DETERMINANTS OF NEOSUBSTRATE SPECIFICITY BEYOND THE G-LOOP

Our current understanding is that the specificity of CRBN-MGD complexes for neosubstrates is in large part governed by the G-loop (16, 17, 19). Beyond the immediate G-loop, however, the interface between CRBN and the neosubstrate that depends on multiple protein-protein interactions also contributes to binding and degradation specificity. For example, two single ZFs, IKZF3 and ZFP91, both engage CRBN-MGD complexes (8) with structurally indistinguishable backbones. If the CRBN-interacting alpha helix of IKZF3 is exchanged with that of ZFP91 (35), a tight binder is obtained (referred to as a superdegron), which is a better degradation target for CRBN-MGD complexes than each of the starting ZFs (8, 35). Placing the helix from IKZF3 into a ZFP91 backbone instead results in a defective ZF (8, 35). The complex protein-protein interactions between CRBN and the entire fold surrounding the G-loop thus also determine specificity (35). Moreover, the interaction between CRBN and additional domains in the neosubstrate, outside the G-loop, further contribute to and tune specificity (8, 16, 17, 35). This applies not only to ZFs but also to other G-loop-containing protein domains that engage CRBN (16, 17). In the CRBN-MGD-CK1 α complex, for example, CK1 α forges additional interactions with the CRBN C-terminal domain by making polar and water-mediated contacts with the CK1 α kinase C-lobe region of the hinge (around residues 144–152 in CK1 α) (16). In the CRBN-CC885-GSPT1 complex, the MGD reaches into the CRBN N-terminal Lon domain, creating an extended neosurface that interacts with the highly conserved GSPT1 C-terminal domain (17) (Figure 1e). However, the CRBN-neosubstrate PPIs are also not the sole determinant of specificity, with neosubstrate binding and degradation further depending on the compound (7, 8, 17, 32). With such complex relationships between the G-loop, MGD, and the remainder of the proteins, how can neosubstrate specificity be rationally engineered through chemical changes in the compound?

TOWARD THE RATIONAL DESIGN OF SELECTIVE DEGRADERS

MGDs often exhibit polypharmacological behavior, degrading multiple proteins. One approach to rationalize MGD specificity is by examining the SAR. As was recently illustrated (36), the

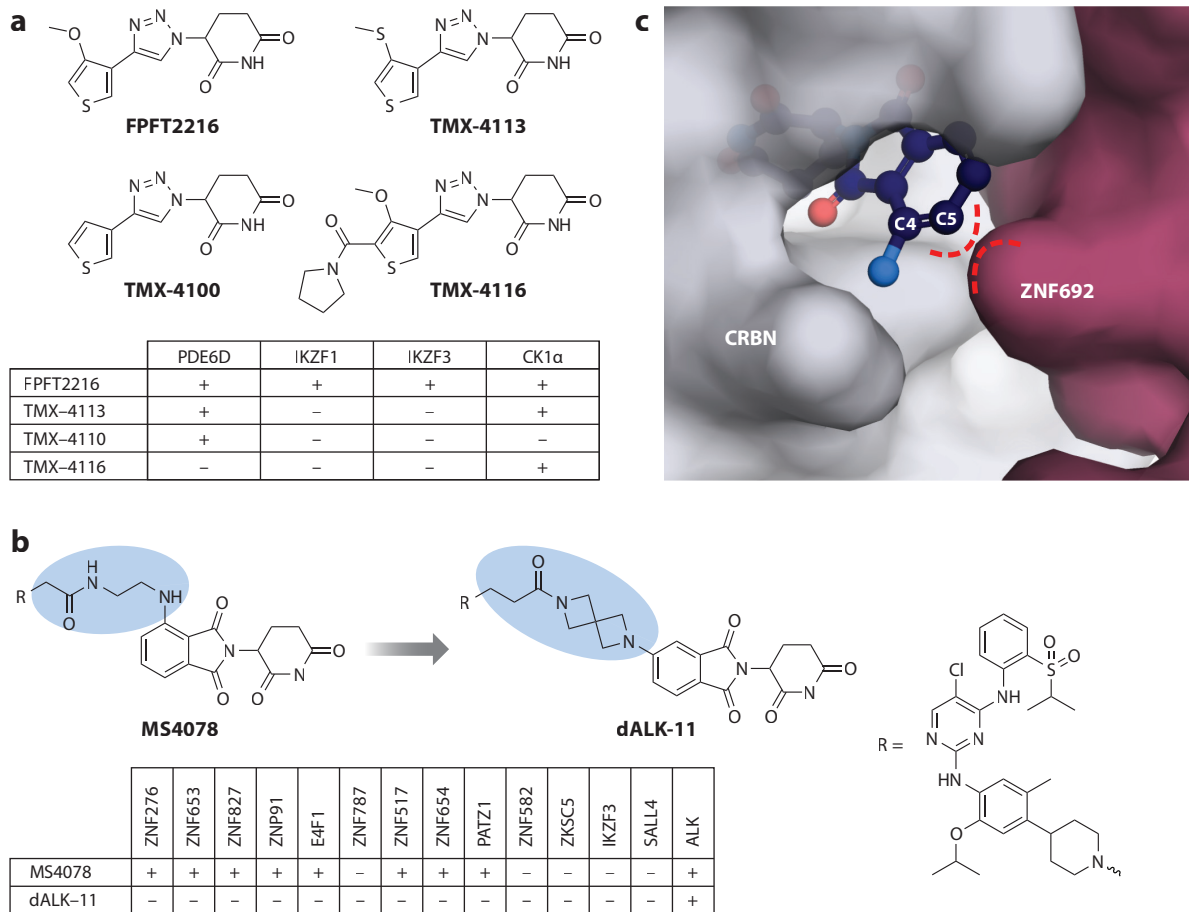


Figure 4

Reported structure-activity relationships to dial in and out neosubstrates. (a) The FPFT2216 series (36). (b) Rational proteolysis-targeting chimera (PROTAC) optimization through changed exit vector and steric/conformational locking of a linker moiety (37). (c) A simple structural explanation for the observed difference in C4 versus C5 exit vector chemistry for thalidomide-based PROTACs illustrated using the CRBN-pomalidomide-ZNF692 complex structure (Protein Data Bank ID 6H0G, <https://www.rcsb.org/structure/6H0G>).

promiscuity of CRBN MGDs can be reduced by minimal compound modification. For example, the promiscuous MGD FPFT2216 targeting PDE6D, IKZF1, IKZF3, and CK1 α , all of which are frequently hit neosubstrates in screens, was transformed into a selective degrader by simple modifications to the FPFT2216 scaffold, yielding the PDE6D-specific compound TMX4100 (**Figure 4a**). As was the case for MGDs targeting ZFs, small modifications in the compound can also radically change the target spectrum for other classes of proteins.

Further insight into chemical tuning of MGDs came from bifunctional degraders, also known as proteolysis-targeting chimeras (PROTACs). PROTAC degraders that use CRBN-engaging components derived from CRBN MGDs, or MGD fragments, have frequently been reported to degrade off-targets through direct, molecular glue-mediated mechanisms. The rules governing the selectivity of PROTACs also yielded important insights for MGD design. To assess the MGD activity of nine reported PROTACs toward ZF proteins, Choudhary and colleagues (37) first

developed an automated imaging assay to profile the ZF degradation spectrum of IMiD derivatives, thus bypassing the need for mass spectrometry-based evaluation of protein degradation. The degrons of 14 known ZF proteins (11 sensitive to pomalidomide and 3 resistant to pomalidomide) were fused with enhanced green fluorescent protein (eGFP) to form a degradation reporter. In the next step, nine reported PROTACs targeting a range of diverse proteins (FKBP12, BRD4, BTK, K-Ras, ALK) were profiled, most of which were shown to significantly degrade several ZF reporter constructs. The most selective compound, MT-802, a BTK-targeting PROTAC, significantly degraded only the ZNF827 degradation reporter. To systematically study the SAR between IMiD functionalization and ZF degradation, a library of 80 thalidomide derivatives was prepared using the C4 and C5 exit vectors (see **Figure 4b,c**) and C-N (S_NAr), N-C (Amidation), and C-C (Suzuki) chemistries. Results of the C-N (S_NAr) sublibrary showed higher selectivity (less ZF reporter degradation) of C5 derivatives compared to analogous modifications at C4. Similarly, compounds lacking an H bond donor (N-H) on the C4 position of the phthalimide ring showed less ZF degradation than their H bond-enabled counterparts. In the crystal structure of CRBN-POM-IKZF1/3 (8), C5 is in tight proximity with the Gln147 residue (at position G-5; see **Figures 1a** and **4b**) of the neosubstrate. Substitution at the C5 position can result in steric clashes with the G-loop. A similar observation was made for C5 substituents in CRBN-POM-ZNF692 [Protein Data Bank (PDB) ID 6H0G], where bulkier functional groups are more likely to clash with a G-loop sidechain residue than substituents on C4 (37). The clashes reduce the target spectrum and offer a rationale for the reduced ZF degradation observed in these PROTACs. Modification at C4, on the other hand, also provides a rationale for the intrinsic promiscuity of pomalidomide-based (i.e., C4-linked) ligands. The most selective PROTAC compounds in this study also all lacked an H bond donor adjacent to the phthalimide ring (at position C4 and C5; see **Figure 4b,c**) and had functional groups mostly at the C5 position. To test the translatability of these observations to PROTAC design, the poorly selective anaplastic lymphoma kinase (ALK) PROTAC MS4078 was modified, and its C4 amino group linker was replaced by a range of ZF-sparing linkers, resulting in 12 new PROTACs. Most of these exhibited reduced or highly reduced degradation of ZFs compared to MS4078, with the compound having a diazasp[3.3]heptane-containing linker in the C5 position, dALK-11, being the most selective (**Figure 4b**). This study highlighted the promiscuity of the thalidomide-based degraders, and a feasible route to restrict off-target activities of PROTACs, while maintaining or improving selectivity for the intended target. The above-described efforts also emphasized the role of the C4 and C5 position in tuning ZF specificity by steric exclusion (**Figure 4c**).

NEW DEGRON, NEW RULES! ENGAGING GSPT1 THROUGH AN EXTENDED CRBN INTERFACE

GSPT1 has recently been identified as a therapeutic target in acute myeloid leukemia (38) and solid tumors (39, 40). The role of GSPT1 in protein synthesis is well understood (41), and its degradation in distinct cancer cell lines leads to easily identifiable cellular phenotypes such as inhibition of proliferation. Structural insight into the CRBN-CC885-GSPT1 ternary complex (17) is available, and diverse compound classes from PROTACs to MGDs have been reported that alter GSPT1 protein levels mediated by CRBN. Yet despite the availability of chemical matter and extensive medicinal chemistry efforts to improve compound binding (42) and GSPT1 degradation, no commonly accepted design rationale has been reported for optimizing a target such as GSPT1.

GSPT1 is not a common off target in the development of PROTACs, in contrast to what was discussed for ZFs above. Nevertheless, the strong cellular phenotypes accompanying GSPT1

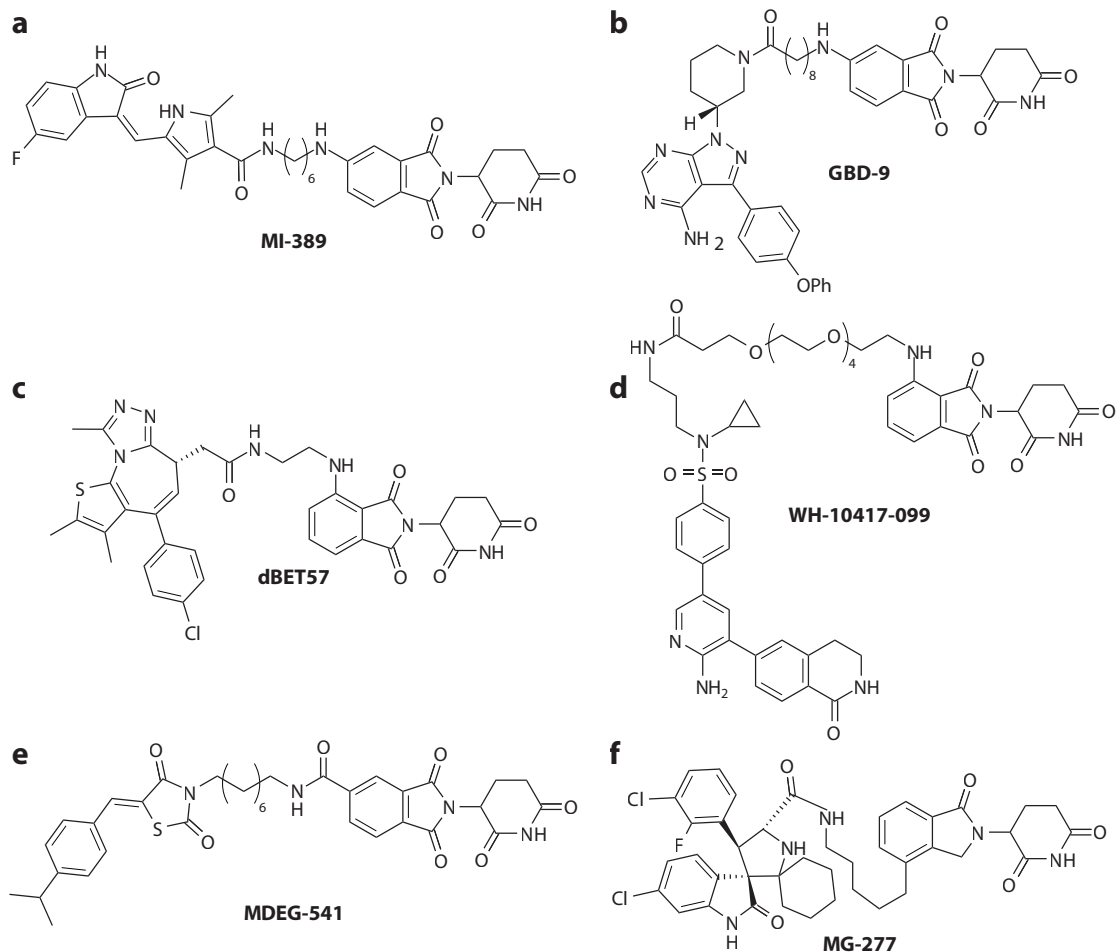


Figure 5

Proteolysis-targeting chimera (PROTAC) entities with pronounced GSPT1 off-target activity described in the literature: (a) MI-389, (b) GBD-9, (c) dBET57, (d) WH-10417-099, (e) MDEG-541, and (f) MG-277.

loss have led to the discovery of GSPT1 degraders. First reports from Winter and colleagues (43) describe the PROTAC MI-389 (**Figure 5a**), based on a C5 amino thalidomide core and the promiscuous kinase inhibitor sunitinib, as an efficient degrader of GSPT1. MI-389 was discovered phenotypically and had its mode of action validated through proteomics experiments. Exchanging sunitinib with ponatinib, while keeping the exit vector geometry and linker length identical (compound 27), resulted in comparable GSPT1 degradation (43). In a similar fashion Rao and colleagues (44) reported a series of C4 and C5 amino thalidomide core and ibrutinib PROTACs, with the C5 amino derivatives such as GBD-9 (**Figure 5b**) being the most efficient GSPT1 degraders. While Winter and colleagues did not observe degradation with any compound employing the C4 exit vector geometry, Rao and colleagues (44) reported compounds with residual activity. Further examples of PROTACs with effects on GSPT1 protein levels can be found in public proteomic databases (45) for dBET57 and WH-10417-099 (**Figure 5c,d**), both comprising a thalidomide core and C4 exit vector geometry. The most recent example was reported by Schneider and colleagues

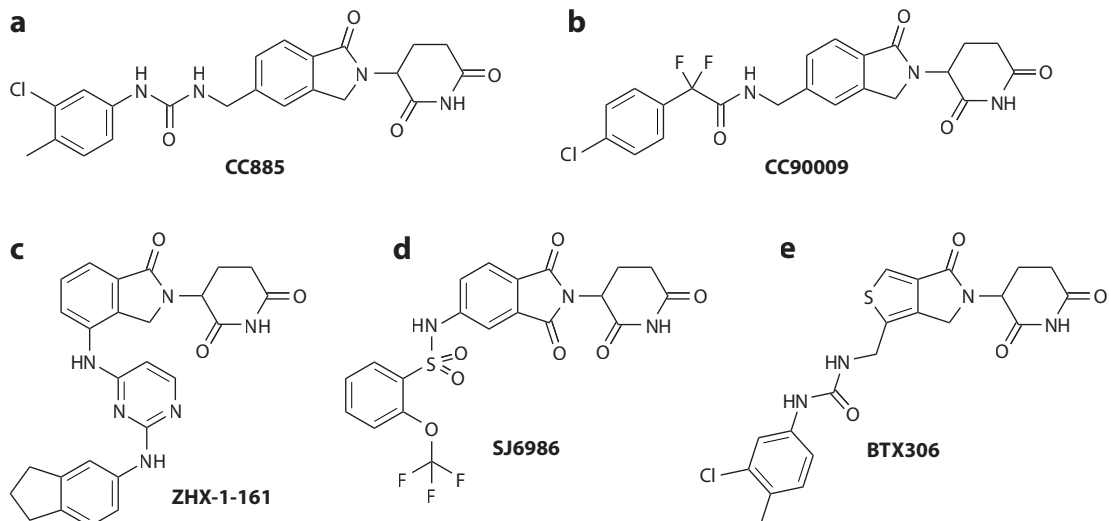


Figure 6

Structures of GSPT1-targeting molecular glue degraders described in the literature: (a) CC885, (b) CC90009, (c) ZHX-1-161, (d) SJ6986, and (e) BTX306.

(46), who investigated different designs for thalidomide-based, MYC-targeting PROTACs and identified MDEG-541 (**Figure 5e**), a potent GSPT1 degrader with a carboxamide linker in the C5 position. Similarly, Wang and colleagues (47) reported MG-277 (**Figure 5f**), an isoindolinone-based PROTAC designed to target MDM2. While MG-277 does not degrade MDM2, it shows a phenotypic activity triggered by GSPT1 degradation. A comprehensive understanding of how these PROTAC molecules induce GSPT1 degradation cannot be derived by examining the existing vectors of the CRBN-binding moiety alone and instead requires considering interactions distal to the G-loop, as is detailed below.

In the field of GSPT1 degraders, novel MGDs are commonly benchmarked to CC885 or CC90009 (**Figure 6a,b**), being the first GSPT1 degrader reported (17) and the first one to enter the clinic (NCT02848001, NCT04336982), respectively. A variety of approaches have been used to identify novel chemical matter and most frequently involve focused libraries followed by phenotypic screens. Fischer and colleagues (48) reported the generation of a thalidomide analog library that delivered selective GSPT1/2 degraders that can spare off targets such as IKZF1/3 (48). The most promising analog, ZHX-1-161 (**Figure 6c**), has a lenalidomide core substituted on the C4 exit vector with an N-linked 2,4-di-amino-pyrimidine ring. Similar to the urea functionality on the C5 exit vector position of CC885, the pyrimidine ring makes an H bond interaction with CRBN His353 facing GSPT1. The model suggested by the authors also implicates the second nitrogen on the pyrimidine in making an H bond interaction with the CRBN Lys628 sidechain. Removing this nitrogen abolishes activity on GSPT1 and confirms that modest electronic variations are not allowed. Similar findings were observed by Rankovic and colleagues (49), who reported the discovery of SJ6986 (**Figure 6d**), a thalidomide core that employs a phenyl sulfonamide to mimic key interactions of CC885 (49). The molecule shows high selectivity for GSPT1 degradation over common off targets. A steep SAR was observed that required an *o*-OCF₃ substituent, highlighting the strict steric requirements for the MGD to form the ternary complex. Moreover, Orłowski and colleagues (50) reported the replacement of the isoindolinone core of CC885 by a thiophene-fused scaffold while keeping the tail constant, which resulted in BTX306 (**Figure 6e**) (50). This

modification in the scaffold only slightly altered the position of the exit vector compared to CC885 and resulted in excellent activity but no enhanced selectivity. This opened the door for further variations at the outer limits of the thalidomide binding pocket (TBP) and presented opportunities for developing novel chemical matter. The first published attempts to rationalize the GSPT1 activity of thalidomide derivatives highlighted the importance of H bonding networks involving CRBN Glu377 (51). This sidechain is preferably engaged via the C5 exit vector and was subsequently suggested to mediate polar interactions with GSPT1 (51). Using the reported CRBN-MGD-GSPT1 X-ray structures for CC885 and CC90009 (**Figure 7a**), it is now possible to further generalize this

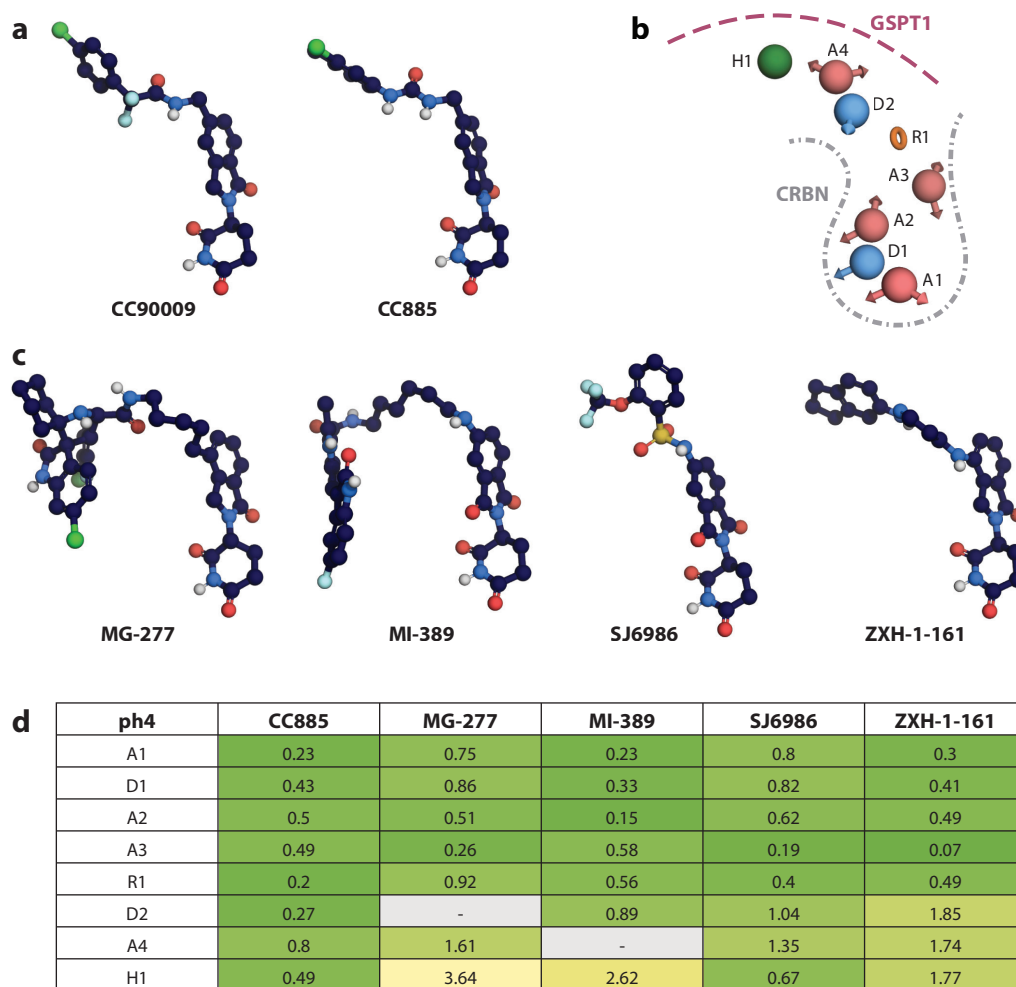


Figure 7

Aligned GSPT1 molecular glue degrader (MGD) structure models. (a) X-ray structures: CC90009 [Protein Data Bank (PDB) ID 6XK9, <https://www.rcsb.org/structure/6XK9>] and CC885 (PDB ID 5HXB, <https://www.rcsb.org/structure/5HXB>). (b) A pharmacophore model based on CC90009: four H bond acceptors in red (A1–A4), two H bond donors in light blue (D1, D2), one aromatic ring in orange (R1), and one hydrophobic moiety in green (H1). (c) In silico models of reported MGDs: MG-277, MI-389, SJ6986, and ZXH-1-161. Panel c adapted from References 43 and 47–49. (d) Nearest pharmacophore distance for each GSPT1 MGD relative to a model based on CC90009 (ph4). Note that H1 may fit rather loosely provided the overall shape of the GSPT1 extended interface is compatible.

observation by defining a consensus pharmacophore set for GSTP1 degraders (**Figure 7b**): Four H bond acceptors (A1–A4), two H bond donors (D1–D2), one aromatic ring (R1), and one hydrophobic moiety (H1) were assigned. Comparing the available models for GSPT1 MGDs by calculating distances to their respective pharmacophores (**Figure 7c**) gave rise to an almost perfect overlay for both ZHX-1-161 and SJ6986. Notably, MI-389 and MG-277 both lack one of the key interactions; either A4 or D2 is missing, with the hydrophobic moiety H1 further away than in the MGDs. As both compounds are still able to induce GSPT1 complexes and drive GSPT1 degradation, the pharmacophore model appears somewhat plastic and will undoubtedly be further refined in the future.

RATIONALIZED DESIGN OF MGDs

To further improve this framework and extend it to other MGD/neosubstrate interactions, it is necessary to consider the immediate environment of the MGD compound. We suggest a simplified concept dividing the surrounding space of the CRBN-bound MGD into three-zones: zone 1, the immediate sphere of the TBP; zone 2, the proximal region beyond the TBP (~ 4.5 to ~ 9.5 Å from the TBP core); and zone 3, the distal sphere (~ 9.5 to ~ 15 Å) (**Figure 8**).

The TBP (zone 1) includes the CRBN tri-Trp cage (Trp380, Trp386, and Trp400) together with surrounding residues Asn351, His357, and His378, as well as part of the alpha-turn (residues G–3 to G+2; see **Figure 1a,c**). Substantial compound modifications are tolerated in zone 1, as lenalidomide, CC122, and FPFT2216 all degrade IKZF1/3 (7, 52) despite having only a glutarimide ring in common (**Figure 9a**). However, some bulkier scaffolds, such as a

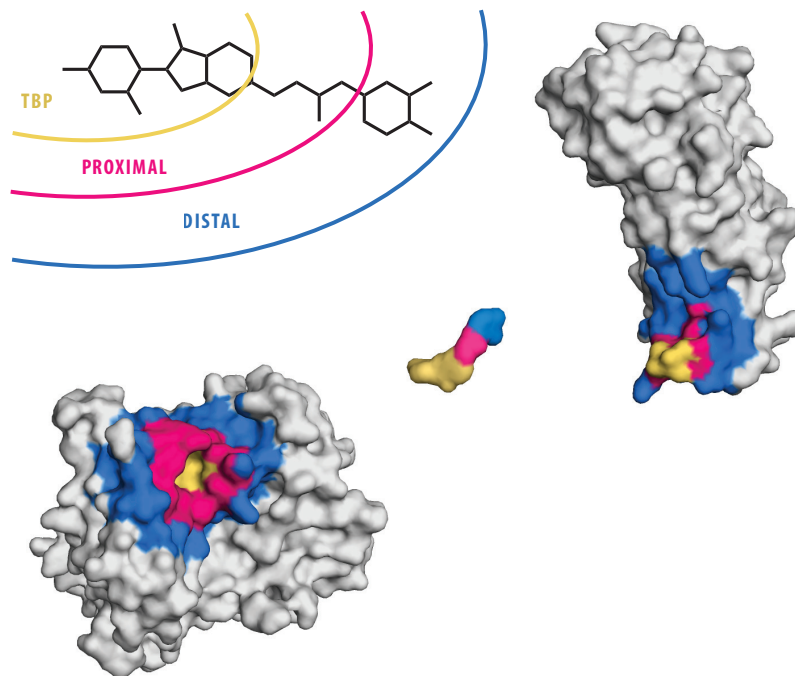


Figure 8

Illustration of the thalidomide binding pocket (TBP) and the proximal and distal spheres. For the CC885 compound, the relative regions are displayed on a 2D structure. The molecular surfaces of cereblon (CRBN) (*left*), CC885 (*middle*), and GSPT1 (*right*) are colored accordingly.

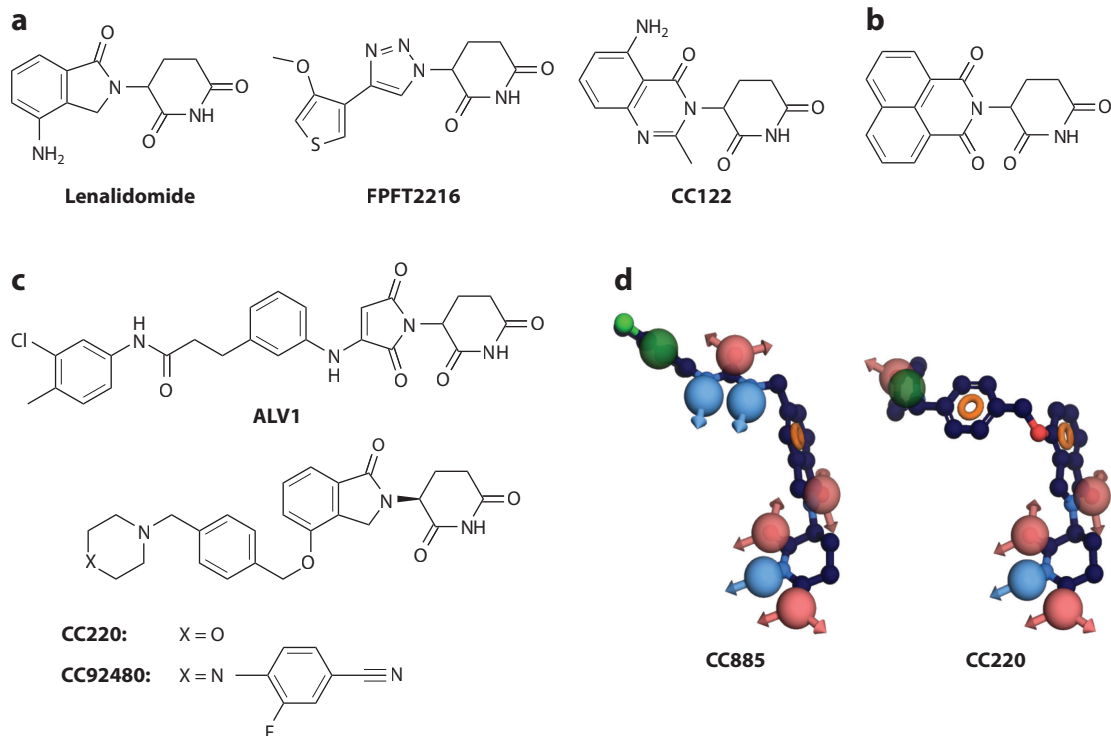


Figure 9

Understanding interactions around the zones. (a) Molecular glue degraders (MGDs) targeting IKZF1/3 have surprisingly little structural similarity but maintain key interactions in zone 1, which explains the shared functional activity. (b) A 1,8-naphthalimide-based thalidomide analog binds the cereblon (CRBN) thalidomide binding pocket but does not degrade IKZF1/3. (c) Highlighted MGDs that extend into zone 3: the IKZF2/4 MGD ALV1 and IKZF1/3 MGDs CC220 and CC92480. (d) Comparison of 3D structures of GSPT1 MGD CC885 [Protein Data Bank (PDB) ID 5HXB, <https://www.rcsb.org/structure/5HXB>] and non-GSPT1 MGD CC220 (PDB ID 5V3O, <https://www.rcsb.org/structure/5V3O>). Although both MGDs occupy a similar space within the distal sphere, their different chemical feature distributions govern their selectivity. H bond acceptors are shown in red, H bond donors are indicated as light blue shapes, aromatic rings are drawn in orange, and the hydrophobic moiety is shown in green.

1,8-naphthalimide-based thalidomide analog (53) (**Figure 9b**) that has been used in PROTACs to remove IKZF1/3 off-target engagement (54), do not degrade alpha-turn targets (53, 54), likely by sterically blocking the interaction. The MGD shape complementarity to CRBN and the G-loop in zone 1 is therefore critical for neosubstrate degradation, yet in isolation, zone 1 is not sufficient for specificity.

Zone 2 coincides with the outer edge of the phthalimide/isoindolinone ring. Substitutions at positions C4 and C5 modulate the interactions with neosubstrate residues near the alpha-turn (in particular, G−5 and G+2) and tune target selectivity. A single-atom change can impact zone 2, as exemplified by a shift in preferred degradation between IKZF1 and SALL4 upon oxidation of thalidomide to 5-hydroxy-thalidomide (21). Analogously, the minimal substitutions on the thiophene ring in the FPFT2216 series tune selectivity for neosubstrates, providing gain/loss of function for CK1α and IKZF1/3. In addition to the G-loop residues, MGDs in the proximal sphere also engage CRBN sidechain residues, notably, Glu377 and His353. These interactions can occur individually, for example, pomalidomide's NH₂ H bond to Glu377 when in complex with ZNF692 (PDB ID 6H0G), or simultaneously, for example, the CC885 urea H bond interactions with Glu377 and His353 (PDB ID 5HXB), and provide affinity as well as selectivity.

RULES FOR CRBN-ENGAGING MGD DESIGN

Rule of Zone 1

MGDs must conserve the interaction within the TBP to maintain efficient CRBN binding, while maintaining a compatible shape to accommodate the key degron motif (e.g., alpha-turn of the G-loop). Provided these two key requirements are met, zone 1 is largely indifferent to target selectivity compared to zones 2 and 3. Depending on the compound scaffold, different substitution vectors will be provided to the proximal sphere (zone 2).

Rule of Zone 2

MGD modifications within the proximal sphere are critical for neosubstrate selectivity. Even a single-atom change in this region impacts target preference through direct interactions with the degron sidechains.

Rule of Zone 3

MGD action, governed by zone 2, can be amplified by compound modifications in zone 3 to enhance CRBN affinity. For neosubstrates that form extended PPIs, MGD modifications that extend beyond the degron into zone 3 also increase activity and selectivity.

Distal interactions in zone 3 occur through residues further away in sequence from the G-loop and thus cannot be readily predicted from sequence alone. Instead, understanding distal contacts requires a reliable surface model of the CRBN-target interface. As illustrated by the CRBN-CC885-GSPT1 structure (**Figure 1a**), distal interactions result in a significantly extended surface, with MGD-neosubstrate interactions reaching beyond 10 Å from the G-loop. The previous section highlighted an example of GSPT1 degraders for which the gain of function required a key hydrophobic contact (H1; **Figure 7b**) between the compound and GSPT1 that falls within this distant region. This example demonstrates that additional specificity can also be achieved through rational modifications in zone 3.

We propose a modular interplay between the zones and formulate a set of design rules for CRBN-engaging MGDs (see the sidebar titled Rules For CRBN-Engaging MGD Design). These rules can be used to further rationalize the reported experimental observations of MGD activity. While a G-loop compatible with Trp-cage binding is necessary, it is not sufficient to degrade the majority of potential neosubstrates. Given the compact nature of the ZF domain, ZF targeting by MGDs largely relies on favorable interactions within the TBP sphere (zone 1). Consequently, interactions within this family of targets tends to be more independent of G-loop sidechains, resulting in more promiscuous ZF targeting.

Neosubstrate selectivity can be tuned by MGD derivatives in the proximal sphere (zone 2) through interactions with the G-loop sidechains facing the TBP. For instance, lenalidomide, a known IKZF1/3 degrader, is unable to degrade a IKZF2/4 ZF2 GFP fusion protein. In contrast, compounds such as CC220 and CC885 that share the same scaffold, while extending into the proximal and distal spheres (zone 2 and 3), show activity against both IKZF1/3 and IKZF2/4 in reporter degradation assays (8, 20). This behavior is also evident for ALV1 where a common isoindolinone core is replaced with anilinomaleimide. There, the available crystal structure (PDB ID 7LPS) reveals that zone 1 contacts are fully maintained, while additional hydrophobic interaction is observed between the His141 sidechain on the IKZF2/4 G-loop and the ethylbenzene moiety of ALV1, rationalizing the improved affinity and specificity over IKZF1/3 (20). Interactions favoring specific neosubstrates can also be acquired by modification in zone 2. This differs from merely blocking unfavorable interactions of a promiscuous initial hit, as discussed previously for

FPFT2216. While all three mentioned MGDs, CC220, CC885, and ALV1, extend to the distal sphere, their X-ray structures (PDB IDs 5V3O, 5HXB, and 7LPS, respectively) leverage CRBN contacts in zone 3, thereby likely increasing CRBN affinity (55, 56). Recently published cryogenic electron microscopy (cryo-EM) structures of CRBN suggest that CC220 and its more elaborate analog CC92480 (**Figure 9c**) amplify their respective activity by stabilizing the CRBN closed conformation (22). This is achieved by the MGD making additional interactions with CRBN's N-Lon domain rather than direct contacts with the IKZF1 neosubstrate (PDB ID 8D7Z). On the other hand, neosubstrates that form an extended interface with CRBN, as evident for CC885 and GPST1, boost both affinity and target specificity through modifications in the MGD distal sphere (zone 3) (17). The MGD GSPT1 proximal region varies in length, substitution vector, and chemical composition, with degradation being additionally driven by distal hydrophobic pharmacophores in zone 3 (**Figure 7**). The importance of chemical composition is demonstrated by degraders CC220 and CC885, both of which occupy similar volumes in zone 3, with distinct pharmacophores (**Figure 9d**). While CC885 is sufficiently complementary to GSPT1 and triggers its degradation, CC220 does not (17, 55).

OUTLOOK AND CONCLUSIONS

The field of targeted protein degradation has left its early days of serendipity-driven discoveries behind, and by revealing the mode of action of MGDs we are now able to define ligase-specific recognition motifs and even mine for these degrons in databases such as AF2. G-loop degrons, recognizable by CRBN-MGD complexes, are the best-described degrons, and their rich abundance in the human proteome opens the door for numerous opportunities in drug discovery. As the CRBN chemical matter evolves, it is likely that many other degron types beyond the G-loop will be recognized, opening the door to even more potential neosubstrates. The appearance of many CRBN-based MGDs and recent progress in understanding and designing specificity for neosubstrate degradation have already established these small-molecule degraders as a stand-alone therapeutic modality, and the available data provide a set of rules rationalizing the observed MGD activity for use in MGD design. As such, we anticipate that the field will produce the next generation of MGD drugs through rational design.

DISCLOSURE STATEMENT

N.H.T. receives funding from the Novartis Research Foundation and is a scientific advisory board member of Monte Rosa Therapeutics and an advisor to Zenith Therapeutics and Ridgeline.

ACKNOWLEDGMENTS

The authors would like to thank Georg Petzold, Owen Wallace, and John Castle for discussions and comments on the manuscript. Work in the Thomä lab (N.H.T.) was supported by the European Research Council (ERC) under the European Union's Horizon 2020 Research and Innovation Program (grant 666068; NucEM, 884331), by 310030_301206, by Krebsliga (KFS 4980-02-2020), by the Swiss National Science Foundation (CRSII5_186230), by SNF 31003A_17954, and by the Novartis Research Foundation.

LITERATURE CITED

1. Silverman WA. 2002. The schizophrenic career of a “monster drug.” *Pediatrics* 110(2):404–6
2. Sampaio EP, Sarno EN, Galilly R, Cohn ZA, Kaplan G. 1991. Thalidomide selectively inhibits tumor necrosis factor alpha production by stimulated human monocytes. *J. Exp. Med.* 173(3):699–703

3. D'Amato RJ, Loughnan MS, Flynn E, Folkman J. 1994. Thalidomide is an inhibitor of angiogenesis. *PNAS* 91(9):4082–85
4. Siegel DS, Schiller GJ, Song KW, Agajanian R, Stockerl-Goldstein K, et al. 2020. Pomalidomide plus low-dose dexamethasone in relapsed refractory multiple myeloma after lenalidomide treatment failure. *Br. J. Haematol.* 188(4):501–10
5. Krönke J, Udeshi ND, Narla A, Grauman P, Hurst SN, et al. 2014. Lenalidomide causes selective degradation of IKZF1 and IKZF3 in multiple myeloma cells. *Science* 343(6168):301–5
6. Lu G, Middleton RE, Sun H, Naniong M, Ott CJ, et al. 2014. The myeloma drug lenalidomide promotes the cereblon-dependent destruction of Ikaros proteins. *Science* 343(6168):305–9
7. Krönke J, Fink EC, Hollenbach PW, MacBeth KJ, Hurst SN, et al. 2015. Lenalidomide induces ubiquitination and degradation of CK1 α in del(5q) MDS. *Nature* 523(7559):183–88
8. Sievers QL, Petzold G, Bunker RD, Renneville A, Słabicki M, et al. 2018. Defining the human C2H2 zinc finger degrome targeted by thalidomide analogs through CRBN. *Science* 362(6414):eaat0572
9. Cao S, Kang S, Mao H, Yao J, Gu L, Zheng N. 2022. Defining molecular glues with a dual-nanobody cannabidiol sensor. *Nat. Commun.* 13(1):815
10. Han T, Goralski M, Gaskill N, Capota E, Kim J, et al. 2017. Anticancer sulfonamides target splicing by inducing RBM39 degradation via recruitment to DCAF15. *Science* 356(6336):eaal3755
11. Shergalis AG, Marin VL, Rhee DY, Senaweera S, McCloud RL, et al. 2023. CRISPR screen reveals BRD2/4 molecular glue-like degrader via recruitment of DCAF16. *ACS Chem. Biol.* 18(2):331–39
12. Bradner J. 2021. *Molecular glues for intractable targets*. Dana-Farber Cancer Inst. Target. Protein Degrad. Semin., Febr. 4. <https://youtu.be/eDZ8UHi1EhI?t=1>
13. Słabicki M, Kozicka Z, Petzold G, Li Y-D, Manojkumar M, et al. 2020. The CDK inhibitor CR8 acts as a molecular glue degrader that depletes cyclin K. *Nature* 585(7824):293–97
14. Kramer LT, Zhang X. 2022. Expanding the landscape of E3 ligases for targeted protein degradation. *Curr. Res. Chem. Biol.* 2:100020
15. Gandhi AK, Kang J, Havens CG, Conklin T, Ning Y, et al. 2014. Immunomodulatory agents lenalidomide and pomalidomide co-stimulate T cells by inducing degradation of T cell repressors Ikaros and Aiolos via modulation of the E3 ubiquitin ligase complex CRL4^{CRBN}. *Br. J. Haematol.* 164(6):811–21
16. Petzold G, Fischer ES, Thomä NH. 2016. Structural basis of lenalidomide-induced CK1 α degradation by the CRL4^{CRBN} ubiquitin ligase. *Nature* 532(7597):127–30
17. Matyskiela ME, Lu G, Ito T, Pagarigan B, Lu C-C, et al. 2016. A novel cereblon modulator recruits GSPT1 to the CRL4^{CRBN} ubiquitin ligase. *Nature* 535(7611):252–57
18. DuPai CD, Davies BW, Wilke CO. 2021. A systematic analysis of the beta hairpin motif in the Protein Data Bank. *Protein Sci.* 30(3):613–23
19. Matyskiela ME, Clayton T, Zheng X, Mayne C, Tran E, et al. 2020. Crystal structure of the SALL4-pomalidomide-cereblon-DDB1 complex. *Nat. Struct. Mol. Biol.* 27(4):319–22
20. Wang ES, Verano AL, Nowak RP, Yuan JC, Donovan KA, et al. 2021. Acute pharmacological degradation of Helios destabilizes regulatory T cells. *Nat. Chem. Biol.* 17(6):711–17
21. Furihata H, Yamanaka S, Honda T, Miyauchi Y, Asano A, et al. 2020. Structural bases of IMiD selectivity that emerges by 5-hydroxythalidomide. *Nat. Commun.* 11(1):4578
22. Watson ER, Novick S, Matyskiela ME, Chamberlain PP, de la Peña AH, et al. 2022. Molecular glue CELMoD compounds are regulators of cereblon conformation. *Science* 378(6619):549–53
23. Hanzl A, Casement R, Imrichova H, Hughes SJ, Barone E, et al. 2023. Functional E3 ligase hotspots and resistance mechanisms to small-molecule degraders. *Nat. Chem. Biol.* 19:323–33
24. Shen C, Nayak A, Neitzel LR, Adams AA, Silver-Isenstadt M, et al. 2021. The E3 ubiquitin ligase component, Cereblon, is an evolutionarily conserved regulator of Wnt signaling. *Nat. Commun.* 12(1):5263
25. Ichikawa S, Flaxman HA, Xu W, Vallavoju N, Lloyd HC, et al. 2022. The E3 ligase adapter cereblon targets the C-terminal cyclic imide degron. *Nature* 610(7933):775–82
26. Gainza P, Wehrle S, Van Hall-Beauvais A, Marchand A, Scheck A, et al. 2023. De novo design of site-specific protein interactions with learned surface fingerprints. *Nature* 617(7959):176–84
27. Donovan KA, An J, Nowak RP, Yuan JC, Fink EC, et al. 2018. Thalidomide promotes degradation of SALL4, a transcription factor implicated in Duane Radial Ray syndrome. *eLife* 7:e38430

28. Jumper J, Evans R, Pritzel A, Green T, Figurnov M, et al. 2021. Highly accurate protein structure prediction with AlphaFold. *Nature* 596(7873):583–89
29. Tunyasuvunakool K, Adler J, Wu Z, Green T, Zielinski M, et al. 2021. Highly accurate protein structure prediction for the human proteome. *Nature* 596(7873):590–96
30. Yamanaka S, Horiuchi Y, Matsuoka S, Kido K, Nishino K, et al. 2022. A proximity biotinylation-based approach to identify protein-E3 ligase interactions induced by PROTACs and molecular glues. *Nat. Commun.* 13(1):183
31. Asatsuma-Okumura T, Ando H, de Simone M, Yamamoto J, Sato T, et al. 2019. p63 is a cereblon substrate involved in thalidomide teratogenicity. *Nat. Chem. Biol.* 15(11):1077–84
32. Matyskiela ME, Zhu J, Baughman JM, Clayton T, Slade M, et al. 2020. Cereblon modulators target ZBTB16 and its oncogenic fusion partners for degradation via distinct structural degrons. *ACS Chem. Biol.* 15(12):3149–58
33. Dunbar K, Macartney TJ, Sapkota GP. 2021. IMiDs induce FAM83F degradation via an interaction with CK1 α to attenuate Wnt signalling. *Life Sci. Alliance* 4(2):e202000804
34. Renneville A, Gasser JA, Grinshpun DE, Jean Beltran PM, Udeshi ND, et al. 2021. Avadomide induces degradation of ZMYM2 fusion oncoproteins in hematologic malignancies. *Blood Cancer Discov.* 2(3):250–65
35. Jan M, Scarfò I, Larson RC, Walker A, Schmidts A, et al. 2021. Reversible ON- and OFF-switch chimeric antigen receptors controlled by lenalidomide. *Sci. Transl. Med.* 13(575):eabb6295
36. Teng M, Lu W, Donovan KA, Sun J, Krupnick NM, et al. 2022. Development of PDE6D and CK1 α degraders through chemical derivatization of FPFT-2216. *J. Med. Chem.* 65(1):747–56
37. Nguyen TM, Deb A, Kokkonda P, Sreekanth V, Tiwari PK, et al. 2021. Proteolysis targeting chimeras with reduced off-targets. bioRxiv 2021.11.18.468552. <https://doi.org/10.1101/2021.11.18.468552>
38. Hansen JD, Correa M, Alexander M, Nagy M, Huang D, et al. 2021. CC-90009: a cereblon E3 ligase modulating drug that promotes selective degradation of GSPT1 for the treatment of acute myeloid leukemia. *J. Med. Chem.* 64(4):1835–43
39. Gavory G, Ghandi M, d’Alessandro A-C, Bonenfant D, Chicas A, et al. 2022. Identification of MRT-2359 a potent, selective and orally bioavailable GSPT1-directed molecular glue degrader (MGD) for the treatment of cancers with Myc-induced translational addiction. *Cancer Res.* 82(Suppl. 12):3929 (Abstr.)
40. Gavory G, Fasching B, Bonenfant D, Sadok A, Singh A, et al. 2021. Identification of GSPT1-directed molecular glue degrader (MGD) for the treatment of Myc-driven breast cancer. *Mol. Cancer Ther.* 20(Suppl. 12):LBA004 (Abstr.)
41. Janzen DM. 2004. The effect of eukaryotic release factor depletion on translation termination in human cell lines. *Nucleic Acids Res.* 32(15):4491–502
42. Kazantsev A, Krasavin M. 2022. Ligands for cereblon: 2017–2021 patent overview. *Expert Opin. Ther. Pat.* 32(2):171–90
43. Ishoey M, Chorn S, Singh N, Jaeger MG, Brand M, et al. 2018. Translation termination factor GSPT1 is a phenotypically relevant off-target of heterobifunctional phthalimide degraders. *ACS Chem. Biol.* 13(3):553–60
44. Yang Z, Sun Y, Ni Z, Yang C, Tong Y, et al. 2021. Merging PROTAC and molecular glue for degrading BTK and GSPT1 proteins concurrently. *Cell Res.* 31(12):1315–18
45. Fischer Lab. 2020. *Fischer lab’s proteomics database*. Database, Dana-Farber Cancer Inst., Boston, MA. <https://proteomics.fischerlab.org>
46. Lier S, Sellmer A, Orben F, Heinzlmeir S, Krauß L, et al. 2022. A novel cereblon E3 ligase modulator with antitumor activity in gastrointestinal cancer. *Bioorg. Chem.* 119:105505
47. Yang J, Li Y, Aguilar A, Liu Z, Yang C-Y, Wang S. 2019. Simple structural modifications converting a bona fide MDM2 PROTAC degrader into a molecular glue molecule: a cautionary tale in the design of PROTAC degraders. *J. Med. Chem.* 62(21):9471–87
48. Powell CE, Du G, Che J, He Z, Donovan KA, et al. 2020. Selective degradation of GSPT1 by cereblon modulators identified via a focused combinatorial library. *ACS Chem. Biol.* 15(10):2722–30
49. Nishiguchi G, Keramatnia F, Min J, Chang Y, Jonchere B, et al. 2021. Identification of potent, selective, and orally bioavailable small-molecule GSPT1/2 degraders from a focused library of cereblon modulators. *J. Med. Chem.* 64(11):7296–311

50. Zou J, Jones RJ, Wang H, Kuitatse I, Shirazi F, et al. 2020. The novel protein homeostatic modulator BTX306 is active in myeloma and overcomes bortezomib and lenalidomide resistance. *J. Mol. Med.* 98(8):1161–73
51. Nowak RP, Che J, Ferrao S, Kong NR, Liu H, et al. 2023. Structural rationalization of GSPT1 and IKZF1 degradation by thalidomide molecular glue derivatives. *RSC Med. Chem.* 14:501–6
52. Gemechu Y, Millrine D, Hashimoto S, Prakash J, Sanchenkova K, et al. 2018. Humanized cereblon mice revealed two distinct therapeutic pathways of immunomodulatory drugs. *PNAS* 115(46):11802–7
53. Burslem GM, Ottis P, Jaime-Figueroa S, Morgan A, Cromm PM, et al. 2018. Efficient synthesis of immunomodulatory drug analogues enables exploration of structure-degradation relationships. *ChemMedChem* 13(15):1508–12
54. de Wispelaere M, Du G, Donovan KA, Zhang T, Eleuteri NA, et al. 2019. Small molecule degraders of the hepatitis C virus protease reduce susceptibility to resistance mutations. *Nat. Commun.* 10(1):3468
55. Matyskiela ME, Zhang W, Man H-W, Muller G, Khambatta G, et al. 2018. A cereblon modulator (CC-220) with improved degradation of Ikaros and Aiolos. *J. Med. Chem.* 61(2):535–42
56. Chamberlain PP, D'Agostino LA, Ellis JM, Hansen JD, Matyskiela ME, et al. 2019. Evolution of cereblon-mediated protein degradation as a therapeutic modality. *ACS Med. Chem. Lett.* 10(12):1592–602
57. Nowak RP, DeAngelo SL, Buckley D, He Z, Donovan KA, et al. 2018. Plasticity in binding confers selectivity in ligand-induced protein degradation. *Nat. Chem. Biol.* 14(7):706–14
58. Sperling AS, Burgess M, Keshishian H, Gasser JA, Bhatt S, et al. 2019. Patterns of substrate affinity, competition, and degradation kinetics underlie biological activity of thalidomide analogs. *Blood* 134(2):160–70
59. Yu HH, Reitsma JM, Sweredoski MJ, Moradian A, Hess S, Deshaies RJ. 2019. Single subunit degradation of WIZ, a lenalidomide- and pomalidomide-dependent substrate of E3 ubiquitin ligase CRL4^{CRBN}. bioRxiv 595389. <https://doi.org/10.1101/595389>
60. Li L, Xue W, Shen Z, Liu J, Hu M, et al. 2020. A cereblon modulator CC-885 induces CRBN- and p97-dependent PLK1 degradation and synergizes with volasertib to suppress lung cancer. *Mol. Ther. Oncolytics* 18:215–25
61. Hao B, Li X, Jia X, Wang Y, Zhai L, et al. 2020. The novel cereblon modulator CC-885 inhibits mitophagy via selective degradation of BNIP3L. *Acta Pharmacol. Sin.* 41(9):1246–54
62. Tochigi T, Miyamoto T, Hatakeyama K, Sakoda T, Ishihara D, et al. 2020. Aromatase is a novel neosubstrate of cereblon responsible for immunomodulatory drug-induced thrombocytopenia. *Blood* 135(24):2146–58
63. Yamamoto J, Suwa T, Murase Y, Tateno S, Mizutome H, et al. 2020. ARID2 is a pomalidomide-dependent CRL4^{CRBN} substrate in multiple myeloma cells. *Nat. Chem. Biol.* 16(11):1208–17
64. Surka C, Jin L, Mbong N, Lu C-C, Jang IS, et al. 2021. CC-90009, a novel cereblon E3 ligase modulator, targets acute myeloid leukemia blasts and leukemia stem cells. *Blood* 137(5):661–77
65. Zhao M, Hu M, Chen Y, Liu H, Chen Y, et al. 2021. Cereblon modulator CC-885 induces CRBN-dependent ubiquitination and degradation of CDK4 in multiple myeloma. *Biochem. Biophys. Res. Commun.* 549:150–56
66. Lin Z, Shen D, Yang B, Woo CM. 2022. Molecular and structural characterization of lenalidomide-mediated sequestration of eIF3i. *ACS Chem. Biol.* 17(11):3229–37